



Erosion resistance of laser clad Ti-6Al-4V/WC composite for waterjet tooling



P.K. Farayibi, J.W. Murray, L. Huang, F. Boud, P.K. Kinnell, A.T. Clare*

Manufacturing Division, Faculty of Engineering, University of Nottingham, University Park, Nottingham NG7 2RD, UK

ARTICLE INFO

Article history:

Received 29 April 2013

Received in revised form 24 July 2013

Accepted 26 August 2013

Available online 4 September 2013

Keywords:

Waterjet

Masking

Laser cladding

Abrasion resistance

Ti-6Al-4V

WC

ABSTRACT

In waterjet operations, milled surfaces are left with some undesirable dimensional artefacts, thus the use of abrasion resistant mask has been proposed to improve the surface quality of machined components. In this study, the erosion performance of laser clad Ti-6Al-4V/WC composite coating subjected to plain water jet (PWJ) and abrasive water jet (AWJ) impacts to evaluate its potentials for use as waterjet impact resistant mask material and coating on components was investigated. Results showed that composite with 76 wt.% WC composition subjected to PWJ and AWJ impacts offered resistance to erosion up to 13 and 8 times that of wrought Ti-6Al-4V respectively. Scanning electron microscopy (SEM) examination of the eroded composite surfaces showed that the erosion mechanism under PWJ impacts is based on the formation of erosion pits, tunnels and deep cavities especially in the interface between the WC particles and the composite matrix owing to lateral outflow jetting and hydraulic penetration. Composite suffered ploughing of the composite matrix, lateral cracking and chipping of embedded WC particles and WC pull-out under AWJ impacts. The composite performance is attributed to the embedded WC particles and the uniformly distributed nano-sized reaction products (TiC and W) reinforcing the ductile β -Ti composite matrix, with its mean hardness enhanced to 6.1 GPa. The capability of the Ti-6Al-4V/WC composite coating was demonstrated by effective replication of a pattern on a composite mask to an aluminium plate subjected to selective milling by PWJ with an overall depth of 344 μm . Thus, composite cladding for tooling purpose would make it possible to enhance the lifetime of jigs and fixtures and promote rapid machining using the water jet technique.

© 2013 The Authors. Published by Elsevier B.V. Open access under [CC BY-NC-ND license](https://creativecommons.org/licenses/by-nc-nd/4.0/).

1. Introduction

Waterjet is a useful machining technique which is able to cut, mill and surface pattern many materials (Momber and Kovacevic, 1999). It can achieve machining speeds higher than competing cutting processes under appropriate conditions, while leaving the cut surface free from thermal damage, recast layer and almost free from burrs. In abrasive waterjet (AWJ) cutting, abrasive particles, typically garnet, are introduced into a mixing chamber by the vacuum created by the speed of jet flow. The water-abrasive mixture passes through a fine, jewel-made orifice to produce a high-speed jet stream. The abrasive particles travelling at approximately 70% of the water velocity within the jet impinge upon the workpiece surface (Roth et al., 2005) and significantly enhance the erosion rate

of the material from the workpiece. For this reason AWJ is typically used for the processing of engineering materials, whereas plain waterjet (PWJ) is used for the cutting of products such as food stuffs, textiles and modelling materials. Despite this PWJ has attracted specialist interest in machining where high integrity is required, such as titanium aluminide (Kong et al., 2010), Al alloys, and Ti and Ni based superalloys (Kong et al., 2011) for aerospace applications. Though PWJ has a reduced material removal rate, added benefits of improved dimensional tolerance, as well as lack of surface contamination via abrasive embedment, and therefore the avoidance of worsened fatigue properties can be achieved.

The mechanism of material removal varies between the processes. It is complex and dependent on the mechanical properties of the workpiece material and the angle of incidence of the abrasive particles (Finnie, 1960; Zheng and Kim, 1996). For ductile materials, a ploughing and cutting action is generally accepted to characterise the removal mechanism (Summers, 1995). Ruff and Wiederhorn (1979) reported that the removal mechanism on ductile materials is dependent on abrasive particle morphology, as spherically shaped particles impinging ductile materials cause ploughing, while angular particles result in cutting action. As particles impinge the surface, an impact crater is formed on ductile

* Corresponding author at: Room A49, Coates Building, University Park, University of Nottingham, NG7 2RD, UK. Tel.: +44 115 951 4109.

E-mail address: adam.clare@nottingham.ac.uk (A.T. Clare).

materials and the displaced crater material, which flows in the direction of the abrasive particle incidence, fractures at high accumulated strain (Karelin et al., 2002). Brittle materials exhibit a more complex removal mechanism, whereby conical, radial and lateral cracks are formed in the region of impression of the abrasive particle, thereby reducing localised strength of the material and promoting further material removal (Chaudhri and Walley, 1978). As a spherical particle strikes a brittle material surface, hertzian (conical) cracks are formed at the edge of contact due to pre-existing flaws in the target material. When the particle impact force at contact exceeds a threshold value which is dependent on the brittle material hardness and fracture toughness, radial and lateral cracks are initiated and propagated to simultaneously degrade the surface strength and enhance erosive wear by chip formation (Ruff and Wiederhorn, 1979). PWJ has attracted less research interest into material removal mechanisms, but some recent work carried out on titanium alloy by Huang et al. (2012) and Kamkar et al. (2013) has determined it is a complex process comprising of plastic deformation, crack initiation, stress wave propagation and micro pit creation, then trans-granular and inter-granular fracture.

Despite the high material removal rate (MRR) of the AWJ process when compared to PWJ, there remain dimensional artefacts associated with the technology, including a tapered kerf and rounding of corners which need to be removed before some parts are introduced to service (Wang and Wong, 1999). Though, at present, new AWJ systems capable of delivering components with notably improved performance are now available on the market (Flow, 2013), the use of reinforced mask as a template is an appropriate method for repetitive operations especially where low cost PWJ/AWJ machinery is in use. Fig. 1 shows a schematic of a convergent kerf taper where the top kerf width, w_t , is greater than the bottom kerf width, w_b , in a through-cut kerf. This low dimensional tolerance limits the process from machining components to a precise geometry. The focussing tube lifetime is also substantially reduced during AWJ operations compared to PWJ which is of particular importance since it represents the most critical aspect of the waterjet system. Inner bore wear of the focussing tube attached to the orifice degrades the jet coherence as well as kinetic energy and is the shortest-lived component (Nanduri et al., 2000), and for this reason, PWJ also may be advantageous.

When waterjet machining, masking can be used to ensure complex geometry can be reproduced. However for machining using hard mask materials, for the mask to be effective, it must be erosion resistant (the mask material should be harder than the workpiece). Hence in this study, an abrasion resistant laser clad is investigated. Previous studies have revealed the potentials of particle-reinforced composite as effective abrasion resistant materials. Wentzel and Allen (1995) subjected cemented WC with different binder phases (Co, Ni, and Cr) to erosion using silica–water slurry, and observed the reduction in erosion loss as composite hardness increases. It was reported that the preferential binder phase followed by WC detachment governs the erosion mechanism. Gant and Gee (2009) later reported that erosion loss has an inverse log-linear relationship with composite hardness. Lathabai and Pender (1995) evaluated the erosion behaviour of alumina-based composite subjected to silicon carbide abrasive slurry jet, and observed that chipping out of lateral cracks, grain boundary cracking, grain pull out and plastic deformation due to repetitive sliding and impact of abrasive particles define the mechanism of this hard composite material. Pugsley and Allen (1999) investigated the erosion resistance of WC-Co sintered composite exposed to abrasive waterjet impacts, and attributed increased erosion resistance to reduction in WC grain size and reduction of the mean free paths between WC particles, which limits the preferential denudation of the binder phase. In addition, Yarrapareddy and Kovacevic (2008) subjected WC nano-particle reinforced Ni-WC composite prepared via laser

based deposition to high velocity AWJ impacts, and reported an enhanced erosion resistance due to the WC nano-sized particles reinforcing the composite matrix. In another complementary study, Castberg et al. (2013) reported that 80% WC size reduction in a Co–Ni–Cr binder phase reduced erosion rate by 30–50%, and maximum erosion rate was observed when the abrasive jet impacts the surface of the composite at 90°. Moreover, for multiphase composite materials subjected to high energy PWJ impacts, Momber and Kovacevic (1996) explained that composite materials fail as a result of micro-crack growth owing to hydrostatic pressure, and particle/matrix interfaces are preferential locations for crack growth, while the particles acts as crack arresters owing to their absorption of the higher amount of the fracture energy. In another study, Shipway and Gupta (2011) investigated the erosion resistance of sintered and thermally sprayed WC-Co composites having subjected them to PWJ impacts, and reported sintered composite exhibited an incubation period during which damage was not experienced, and composite with smallest particle size and higher fraction exhibits the highest resistance, which further support the works of Pugsley and Allen (1999) and Gant and Gee (2009). All the studies showed that particle reinforced composites are suitable candidate materials against wear and erosion.

The previous studies have concentrated on investigating the erosion resistance of WC–Ni, Co, and Cr-based composites prepared by sintering and thermal spraying. However, laser based deposition processes are capable of producing hard-facing composites directly on engineering components and these composites produced have received little attention by researchers in the area of their erosion resistance characterisation under high energy jet impacts. Moreover, the characterisation of WC–Ti based composite subjected to high energy PWJ and AWJ impacts is yet to be investigated.

Laser cladding is an additive manufacturing technique that is capable of depositing a strong metallurgically bonded coating, with several hundred microns to many centimetres layer thickness by repeated application (Ion, 2005). The ability to automate control of the laser/material feed system, precise thermal energy dosing and coating integrity, gives laser cladding advantages over such processes as High Velocity Oxy-Fuel (HVOF) and Cold Spray for precision coatings (Toyserkani et al., 2005). In laser cladding, a wide range of materials can be bonded using a powder-fed or wire-fed system, or a combination of both.

In this study, a clad consisting of a Ti–6Al–4V matrix and WC particles will be investigated for its abrasion resistance to AWJ and PWJ. Previous studies have shown that using a pre-blended powder of these two materials can produce a crack-free, non-porous clad with a uniform distribution of WC particles, exhibiting slurry abrasion wear behaviour seven times that of the titanium alloy substrate (Farayibi et al., 2011). In an early work of Ayers (1984) the wear behaviour of aluminium and titanium alloyed surfaces with TiC and WC particles prepared via laser melt injection process and subjected to dry sand rubber wheel wear test was investigated. His result showed that erosion resistance of Ti–6Al–4V with embedded carbide particles increases as carbide particle size decreases with maximum wear improvement ratio of 13 observed when 50 μm size carbide particles was employed and noted that WC is more effective than TiC in abrasion wear. In another study, Folkes and Shibata (1994) observed an enhanced hardness of Ti-based composite matrix prepared via laser cladding of Ti–6Al–4V with different carbide powders and it was noted that the composite containing WC particles has the highest hardness value of 500 HV which slightly decrease with increasing temperature. Also, Vreeling et al. (2002) studied the pin-on-disc wear behaviour of Ti–6Al–4V surface strengthened with WC particles via laser melt injection process and noted a significant improvement in wear performance of the strengthened Ti–6Al–4V compared to virgin Ti–6Al–4V with specific wear rates of 0.5E–6 and 269E–6 mm^3/Nm respectively

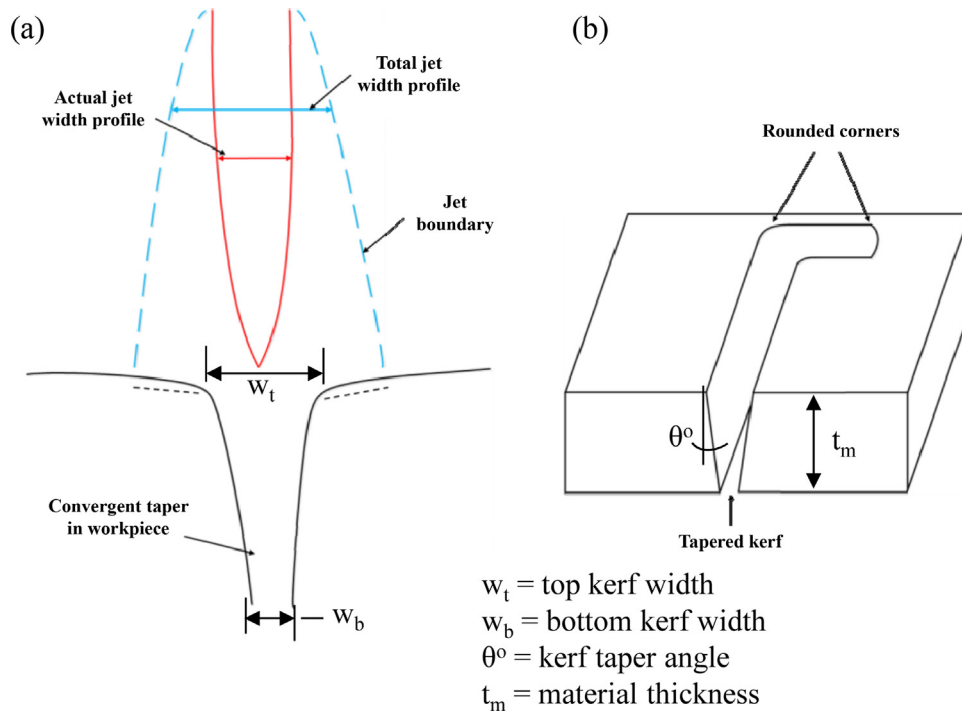


Fig. 1. (a) Schematic showing divergent jet profile and resultant tapering on workpiece and (b) a typical tapered kerf and rounded corners after AWJ.

reported. Chen et al. (2008), as well, reported an hardness value of 540 HV for the top region of WC/Ti-6Al-4V composite layer prepared via laser melt injection process and attributed the increased hardness to the formation of reaction products (TiC and W) in the matrix. Thus, Ti-6Al-4V can be successfully strengthened with WC particles in such a composite microstructure, and by this method the low density as well as corrosion and high temperature strength of the titanium binder can be exploited. In this study, area clads are produced by simultaneous feeding of WC powder and Ti-6Al-4V wire into a laser generated melt pool on a Ti-6Al-4V substrate. The use of Ti-6Al-4V in wire form is of potential economic importance, as this material utilisation would approach 100%. Also, feeding Ti-6Al-4V wire into the melt pool allows for microstructural flexibility, as the percentage composition of the clad layer can be effectively modified.

Microstructural evolution and hardness of clads produced using a variety of laser processing conditions are investigated. The erosion performance and surface profiles of clads under varying conditions for both AWJ and PWJ are to be measured and compared with those of wrought Ti-6Al-4V erosion. The surface abrasion characteristics will also be investigated and a masking operation with the abrasion resistant coating demonstrated.

2. Experimental

2.1. Equipment and materials

The laser cladding procedure was performed using a 2 kW IPG Ytterbium-doped CW fibre laser operating at a wavelength of 1070 nm, with a beam delivery system consisting of a 125 mm collimating lens and a 200 mm focusing lens. A Precitec YC 50 cladding head with a front feeding nozzle was used for wire delivery coupled with a Redman wire feeder mechanism (Redman Control and Electronics Ltd., England) and a rear feeding nozzle for powder delivery coupled with a model 1264 powder feeder (Praxair Surface Technologies). A 4-axis CNC table was used to automate the traverse of the workpiece while the laser remained stationary. The cladding process was conducted in an inert

chamber which was continuously flushed with argon gas before the start of deposition and through the process to inhibit oxidation.

A schematic of the cladding process with overlap strategy can be seen in Fig. 2. All single tracks to create the area clad began and finished at the same end. A 60% overlap of bead width, W , was chosen in order to minimise the trough regions from the tops of the clad and also not create a clad of increasing thickness in the overlap direction. For each parameter set, as discussed in Section 2.2, ten single tracks were deposited using the overlap procedure outlined in Fig. 2(b).

Waterjet machining was carried out using an Ormond 5-axis AWJ system, equipped with a KMT Streamline SL-V100D ultra-high pressure intensifier pump. It has 100 Horsepower with a water pressure of up to 414 MPa. The jet velocity is 700–1000 m s^{-1} , depending on pressure and orifice used. The cutting head uses ruby orifice with hole diameter of 0.3 mm and includes a Rotec 100 tungsten carbide round-jet focusing tube, with dimensions 1 mm in bore diameter and 76 mm in length. Australian GMA garnet (Almandite) abrasive particles of size range 150–300 μm (80 mesh) were used. Tungsten carbide used in this study was supplied as Spherotene powder by Technogenia (France), and the titanium alloy was supplied as Ti-6Al-4V grade 5 wire by VBC Group (Loughborough, UK).

Profilometry was performed with a Talysurf CLI1000 profilometer with a laser displacement sensor, lateral resolution 1 μm . A central section of each waterjet track was used for these measurements as start and end sections of the tracks were not entirely uniform sure to acceleration and deceleration of the jet. The mean profile of the cross-section of each track obtained was used to calculate the material volume removal rate. The mean profile was determined by the average of 30 scans with a pitch of 200 μm . The surface roughness R_a along the bottom of each track was measured with a sampling length of 3 mm and a cut-off length of 0.8 μm .

2.2. Cladding parameters and microstructure

The cladding experiment was carried out using the laser cladding setup shown in Fig. 2(a). The laser beam has a Gaussian

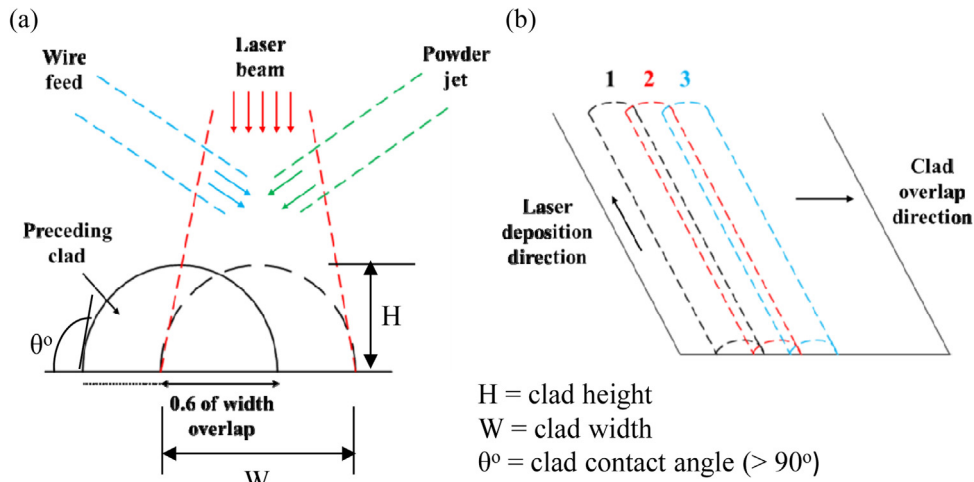


Fig. 2. Schematic of (a) laser cladding process and (b) overall cladding strategy.

profile and was defocused to give a 7.5 mm² circular spot area, to accommodate materials injected into the laser generated melt pool on a Ti-6Al-4V substrate of dimensions (180 mm × 100 mm × 5 mm). The melt pool was simultaneously fed with a 1.2 mm diameter Ti-6Al-4V wire and spherical WC powder with particle size range of 40–270 μm and a mean size of 130 μm determined by laser diffractometry. The feedstocks were delivered continuously as the CNC table traverses to achieve a deposit of Ti-6Al4V/WC composite. The area clads were prepared to achieve high-reinforcement of the Ti-6Al-4V binder matrix as required, and therefore maximum WC content in the binder was targeted. To achieve this, a series of preliminary experiments were performed using a Taguchi design of experiments, under which the parameters: laser power, traverse speed, wire feed rate and powder feed rate were investigated for their main effect on maximum bead height and width and % composition of WC. Table 1(a) summarises the process parameters employed in this study to achieve consistent deposits of single beads with 80 mm length. After the single bead deposition, characterisation was conducted to investigate their WC weight composition. It is anticipated composite beads with highest fraction of WC composition will have the best erosion performance. Thus, Table 1(b) gives the set of process parameters determined by this investigation, which are capable of producing a clad with more than 65% weight WC in the titanium matrix according to studying single composite bead in cross-section.

Fig. 3 shows the cross-sectional microstructures of the clads using the process parameters in Table 1(b). All clads possess a uniform distribution of WC particles. Inter-run pores were not observed in set A, suggesting this set of parameters is ideal to

produce a dense coating, while only a few pores were seen in set B and set C. The clads were metallurgically bonded to the substrate and no cracks were observed at the fusion zone and in the clad coating, except at the top region of set A clad, where few cracks were seen and were eliminated after surface grinding. This suggests that 75 wt.% WC may be the threshold percentage of reinforcement particles allowable in Ti matrix, thus, an attempt to have higher than this percentage would result in cracks formed in the deposit. Since undulation is observed at the tops of all area-clads due to the overlapping process, all specimens were ground to result in a flat clad surface ideal for comparison of erosion performance with that of bulk Ti-6Al-4V.

2.3. Waterjet parameters and strategy

The waterjet experiments were first carried out using PWJ on the ground clad and substrate-only surfaces. The most resistive composite layer under PWJ erosion was then investigated for its performance under AWJ machining. Given the absence of AWJ cutting information for Ti-6Al-4V/WC composite, the selection of processing parameters was based on prior knowledge on the cutting of Ti-6Al-4V alone. The final parameters for both PWJ and AWJ can be seen in Table 2. For the cutting strategy, on both the laser-deposited Ti-6Al-4V/WC composite and Ti-6Al-4V substrate a series of single tracks were machined from the ground surfaces of deposited Ti-6Al-4V/WC composite using all combinations of process parameters shown in. The jet traverse path length was 18 mm; and the spacing between each track was 3.5 mm.

Table 1

(a) Process parameters for single bead deposition. (b) Cladding parameter employed to prepare area clads.

(a)Parameter	Value				
Laser power, W	1400–1600–1800				
Traverse speed, mm/min	200–300–400				
Wire feed rate, mm/min	700–750–800				
Powder feed rate, g min ⁻¹	10–20–30				
Carrier gas flow rate, l min ⁻¹	10				
Shielding gas flow rate, l min ⁻¹	30				
(b)Set	Laser power (W)	Traverse speed (mm/min)	Wire feed rate (mm/min)	Powder feed rate (g min ⁻¹)	WC composition (wt.%)
A	1800	300	700	30	76 ± 1
B	1600	200	750	30	74 ± 2
C	1400	400	800	30	68 ± 2

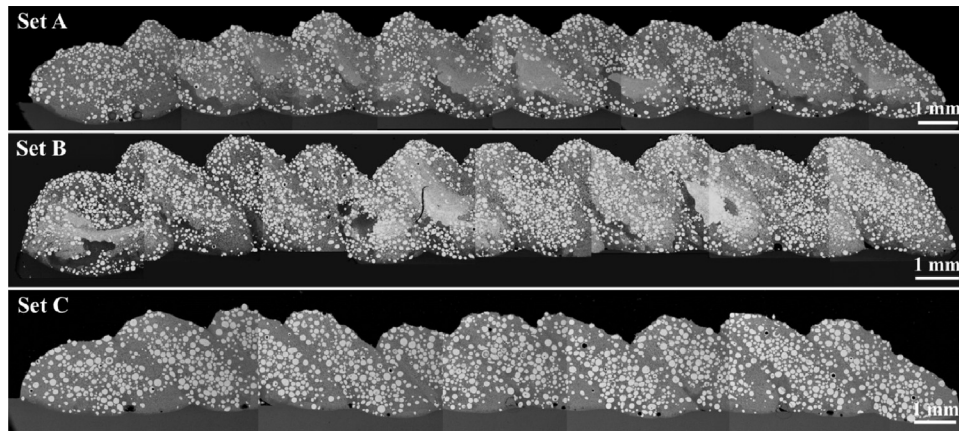


Fig. 3. Cross-sectional microstructures of dissected area-clads using the 3 final experimental parameters.

3. Results and discussion

3.1. Hardness evolution

Fig. 4(a) shows the microhardness variation across the bead cross section. The Vickers hardness test was conducted using a load of 300 g (2.94 N) and a loading time of 15 s. The indentations were made at 120 μm intervals from the top of the clad cross section down into the substrate. Embedded WC particles were avoided to prevent distortion of the hardness profile. The hardness of regions which are a mixture of TiC and W solid solution precipitates in the β -Ti solid solution have hardness values which lie between 5 and 7.7 GPa, and the mean hardness of the composite matrix was calculated as \sim 6.1 GPa. The fusion zone which is in the melt pool depth region has a mean hardness of 4.5 GPa. The recrystallised region of the substrate in the heat affected zone (HAZ) has a mean hardness of 3.8 GPa, which is slightly higher than that of the unaffected region of the substrate with a mean hardness of 3.4 GPa. The clad matrix hardness is enhanced by the uniform distribution of the reaction products (TiC and W) in the β -Ti solid solution (Chen et al., 2008; Farayibi et al., 2013).

Fig. 4(b) shows a hardness indent in region near the embedded WC particle. The hardness value at this point is 7.7 GPa. The increased hardness in the WC-near region in the clad matrix is due to localised diffusion and microstructure modification around the particles. The reduction of hardness in the fusion zone may be attributed to increased concentration of titanium in this region. The localised metallurgical change in the heat affected zone due to rapid cooling is responsible for increased hardness over that of the measured Ti-6Al-4V substrate which is similar to expected values for the material (3.4 GPa) (Welsch et al., 1994).

3.2. Erosion rate under PWJ

Fig. 5 shows the erosion rate of Ti-6Al-4V and Ti-6Al-4V/WC composites as a function of the jet traverse speed during PWJ

machining at pressures of 275 MPa and 345 MPa. Slower traverse speed indicates longer exposure time and hence greater energy density at the workpiece surface.

It can be seen that for all materials, the erosion rate increases with the decreasing traverse speed of the jet as expected. As the jet traverse speed increases (i.e. the exposure time decreases), the difference between the erosion rates of Ti-6Al-4V and Ti-6Al-4V/WC composite layers becomes insignificant at a lower pressure. It was evident that the Ti-6Al-4V/WC composite processed by laser-deposition parameter set A exhibits the best erosion resistance as the erosion rate was minimised for both pressures and all traverse speeds. Also, it can be seen that the difference in erosion rates of the Ti-6Al-4V and the Ti-6Al-4V/WC composite decreases as the traverse speed increases.

The erosion damage experienced by the Ti-6Al-4V/WC composites under PWJ impacts must have resulted from direct deformation, stress wave propagation, lateral outflow jets, and hydraulic penetration (Adler, 1979). As the high velocity PWJ exit from the nozzle, the jet is atomised into water droplets due to its aerodynamic interaction with surrounding air medium (Leu et al., 1998). Field (1999) explained that the water droplets behave in an incompressible manner and on impact with the solid surface result in a high pressure known as water-hammer pressure which can be derived from Eq. (1).

$$P_h = \frac{1}{2} \rho_0 v_0^2$$

$$P_w = 0.78 c_s \rho_0 v_0$$

$$c_s = c_0 + k(0.78 v_0) \quad (1)$$

where, P_h is pressure head (Pa), ρ_0 is density of water (998 kg m^{-3}) at normal temperature and pressure, v_0 is jet velocity at orifice exit, P_w is water hammer pressure, (Pa), and c_s is shock velocity in the water droplet, c_0 is the acoustic velocity in water at normal temperature and pressure (1480 m s^{-1}), k is a constant with a value of 2 for

Table 2
Waterjet parameters.

PWJ	Head pressure (MPa)	275, 345	
	Traverse speed (mm/min)	20, 50, 100	
	Stand-off distance (SOD) (mm)	3	
	Impingement angle	90°	
AWJ		Set 1	Set 2
	Pressure (MPa)	207	138
	Abrasive feed rate (g/s)	0.39	0.39, 0.92
	Impingement angle (°)	90	90
	Stand-off distance (mm)	3, 10	3
	Traverse speed (mm/min)	50, 100, 200, 500, 1000	50, 100, 200, 500, 1000

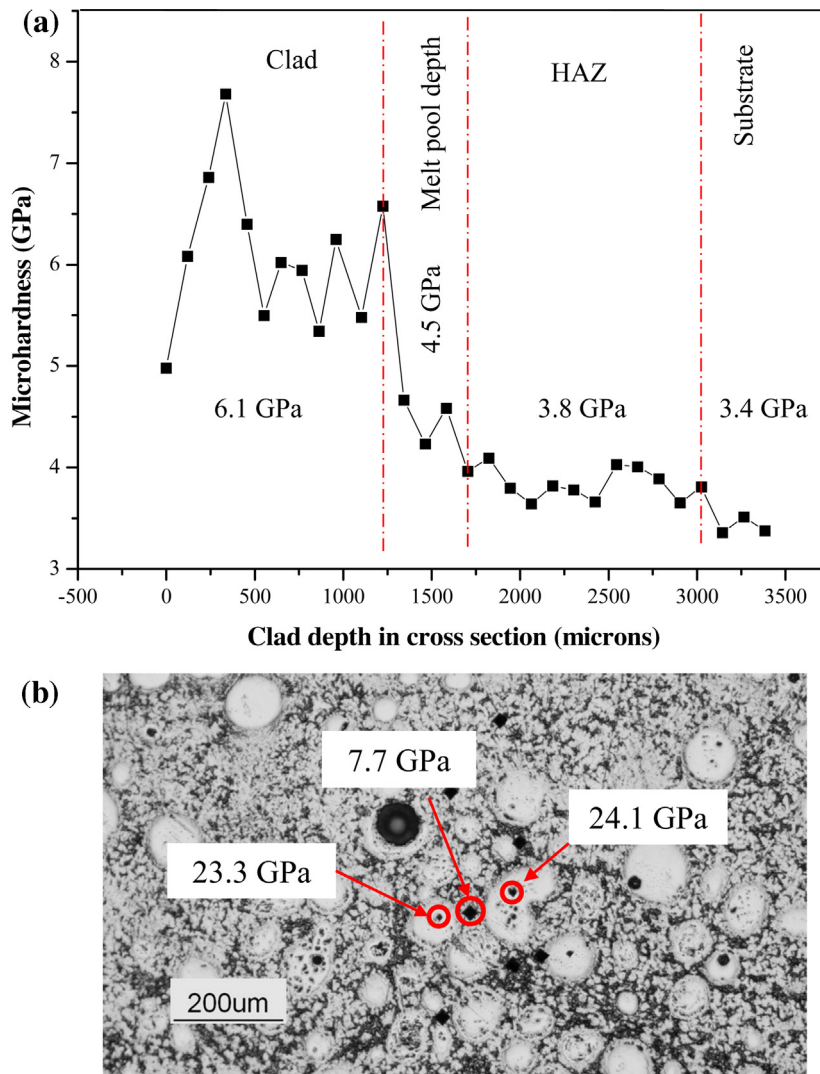


Fig. 4. Hardness variation with depth into the clad under laser parameter set A.

water jet in a velocity range up to 1000 m s^{-1} and the jet velocity coefficient at nozzle exit due to viscosity and turbulence is taken as 0.78 (Huang et al., 2012).

Thus, erosion damage caused by this water hammer pressure is dependent on the material response, as in the case of Ti-6Al-4V/WC composite, the reinforcing WC particles have an elastic–brittle response, while the β -Ti binder phase is expected to respond in a plastic deformation manner as a ductile material. Fig. 6 shows the micrographs of the damage associated with the PWJ impact on the Ti-6Al-4V/WC composite set A. The composite surface was characterised by erosion pits, tunnels and deep cavities generated by lateral outflow jetting and hydraulic penetration. The WC/Ti matrix interface characterised by TiC reaction layer experienced severe pitting and tunnelling due to poor solubility and bonding strength between a WC–TiC system (Upadhyaya, 1998) and was preferentially denuded by lateral outflow jetting which favours subsequent removal of the WC particles (Momber and Kovacevic, 1996).

The interaction of the stress wave and lateral outflow jetting with surface asperities and micro-surface cracks is responsible for the fractures seen on the WC particle (Adler, 1979). The composite matrix also contributed to the enhanced erosion resistance due to the nano-sized TiC and W solid solution precipitates which reinforced the β -Ti phase to increase its hardness as Yarrapareddy and Kovacevic (2008) and Castberg et al. (2013) have reported

the significance of nano-sized reinforced particles and increased hardness to enhanced erosion performance. Though, all the Ti-6Al-4V/WC composites have a significant erosion performance compared to the virgin Ti-6Al-4V, it is worthy to note the composite set A, which had the highest WC composition (Table 1(b)), has the best erosion resistance followed by set B while composite set C had the least erosion resistance both at water hammer pressures of 1.52 GPa and 1.8 GPa resulting from applied pressure heads of 275 MPa and 345 MPa respectively. This complements the significance of high reinforcement particle fraction in composite matrix to better erosion resistance reported by Shipway and Gupta (2011). The overall performance of the composite to wrought Ti-6Al-4V under PWJ was significant due to the embedded WC particles and the reaction products uniformly distributed in the β -Ti matrix.

3.3. Erosion rate under AWJ

From the results of PWJ erosion trials, the Ti-6Al-4V/WC composite processed using the laser-deposition parameter set A has been considered as the most robust masking materials under PWJ impingement. Thus, AWJ machining trials were carried out on this composite as well as Ti-6Al-4V (which is proposed as the machining target material) in order to investigate its potential as a masking material to be used in AWJ processes.

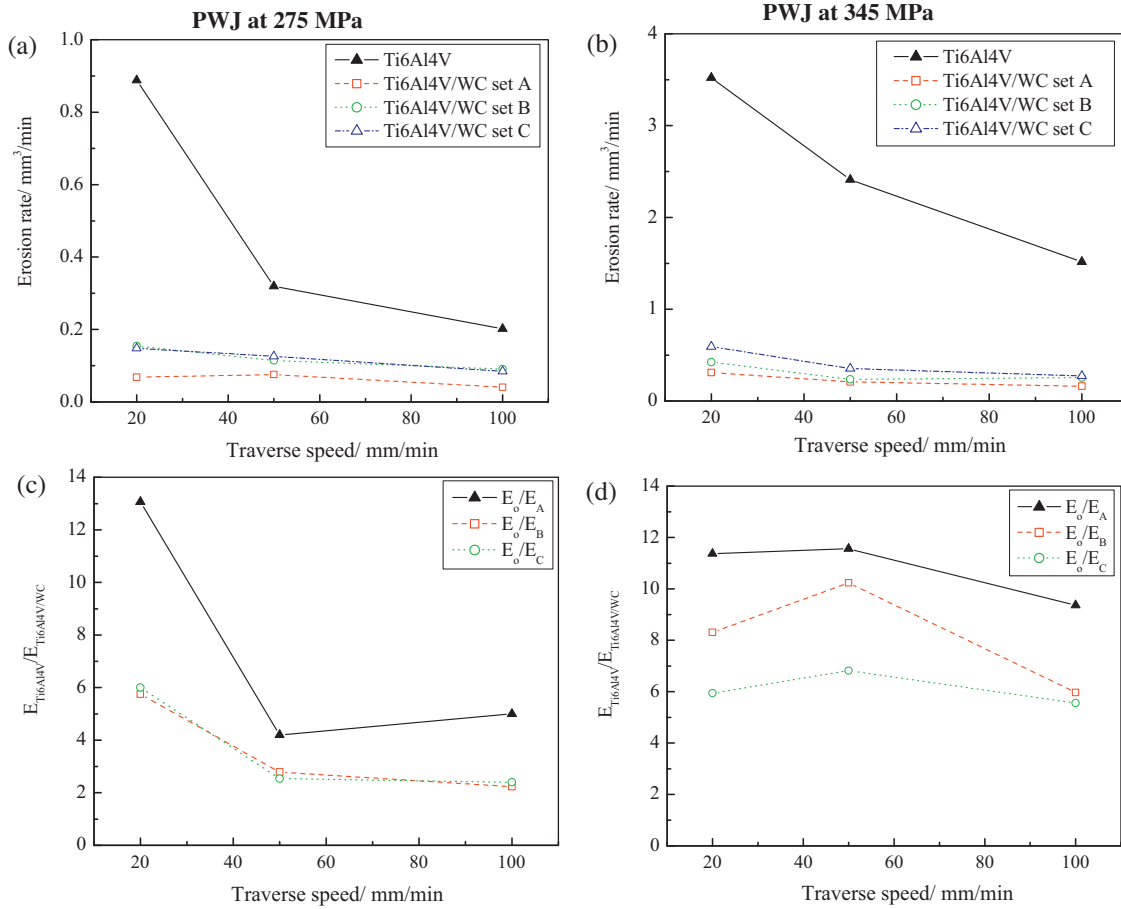


Fig. 5. Erosion rate of composite using PWJ at pressures (a) 275 MPa, (b) 345 MPa, and erosion rate ratio of substrate (E_s):composite (E_c).

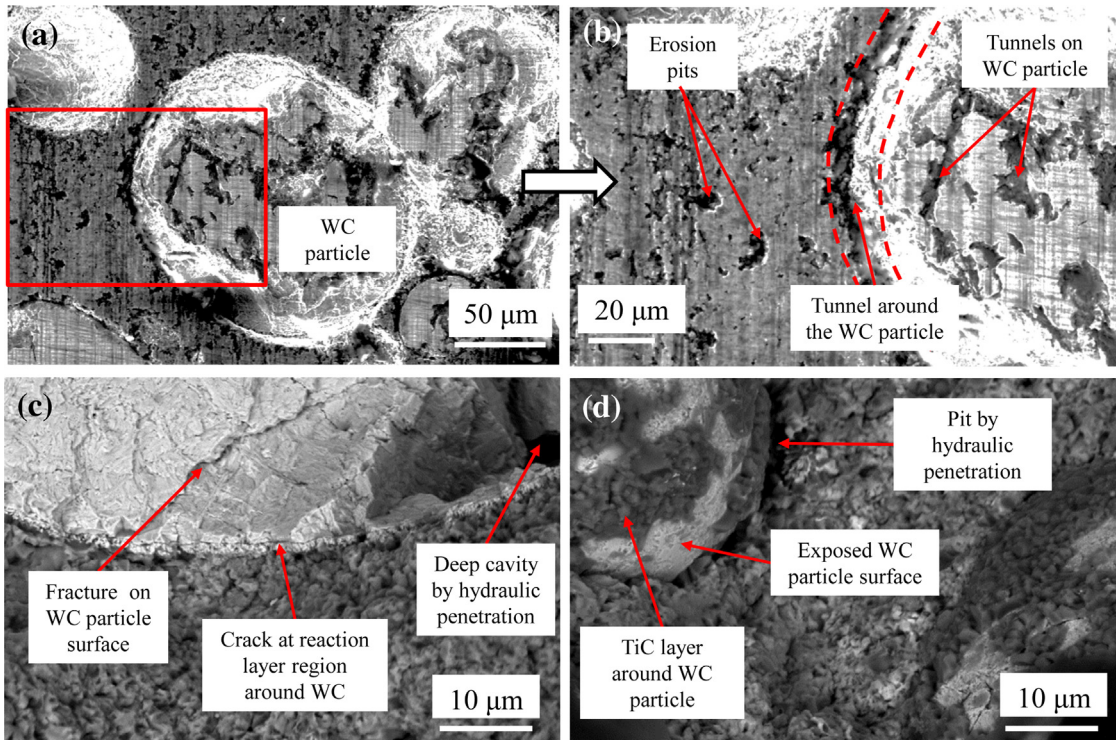


Fig. 6. Micrographs of PWJ impact damage on Ti-6Al-4V/WC composite set A with (a) and (b) obtained from surface treated with 275 MPa pressure, 100 mm/min traverse speed; (c) and (d) 345 MPa pressure, 100 mm/min traverse speed.

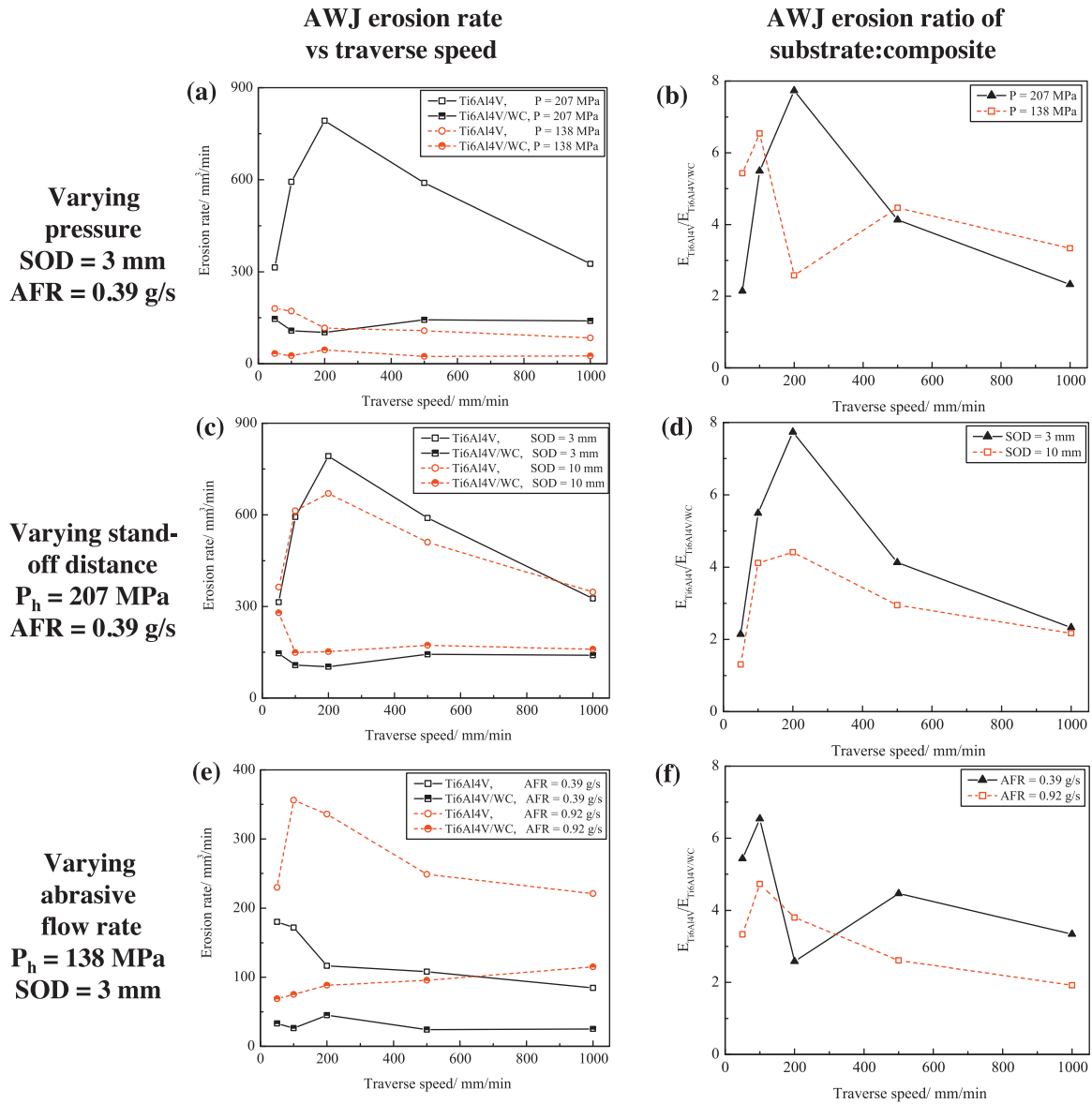


Fig. 7. Erosion rates and ratio of substrate:composite against traverse speed for varying pressure, stand-off distance and abrasive flow rate.

Fig. 7(a) compares the erosion rate of Ti-6Al-4V and the proposed composite under AWJ impingement at different pressures. More prominent differences in erosion rates of the two materials were observed at higher pressures. The change of erosion rate with increasing traverse speed (or decreasing exposure time) can be explained by the well-known erosion-exposure time curve in waterjet erosion (Adler, 1979). The normalised erosion rate (the ratio of erosion rate of Ti-6Al-4V to the erosion rate of the Ti-6Al-4V/WC composite) is shown in Fig. 7(b). The maximum ratio is ~8, resulting from AWJ machining at pressure of 207 MPa and traverse speed of 200 mm/min. Both Fig. 7(a) and (b) suggest that the composite performance is influenced by the machining parameter due to the diverse responses of the composite material and the target material under AWJ impingement.

Fig. 7(c) shows the erosion rate of Ti-6Al-4V and Ti-6Al-4V/WC composite as a function of jet traverse speed for two applied standoff distances, while the normalised erosion rate is shown in Fig. 7(d). Again, the graphs suggest that there is an optimum jet traverse speed (i.e. 200 mm/min) which results in the most significant difference in erosion rate between the proposed masking material and Ti-6Al-4V. Fig. 7(d) indicates that a lower standoff distance lead

to a higher normalised erosion rate. Fig. 7(e) compares the erosion rate of Ti-6Al-4V and Ti-6Al-4V/WC composite during AWJ machining using different abrasive flow rates. Similarly, the erosion rate of Ti-6Al-4V reached a maximum value at the traverse speed of 200 mm/min, resulting in the highest normalised erosion rate. The lower abrasive flow rate generally led to greater differences in erosion rate between the two investigated materials.

The results shown above indicate that there is an optimum jet traverse speed which results in the best erosion performance (lowest normalised erosion rate) for the proposed masking material during AWJ machining. It should be noted that the erosion rate of the masking material was less influenced by the investigated AWJ parameters than that of the Ti6Al4V; and high levels of the normalised erosion rate were always associated with high erosion rates of the supposed machining target (i.e. Ti-6Al-4V). Thus, it is proposed that the performance of a masking material is not only dependent on the erosion rate itself, but also determined by the masking-target materials combination as well as the AWJ parameters used in the machining process. Although, the erosion rate of the proposed Ti-6Al-4V/WC composite can be as low as 1/8 of that of Ti-6Al-4V during AWJ machining, the AWJ resulted

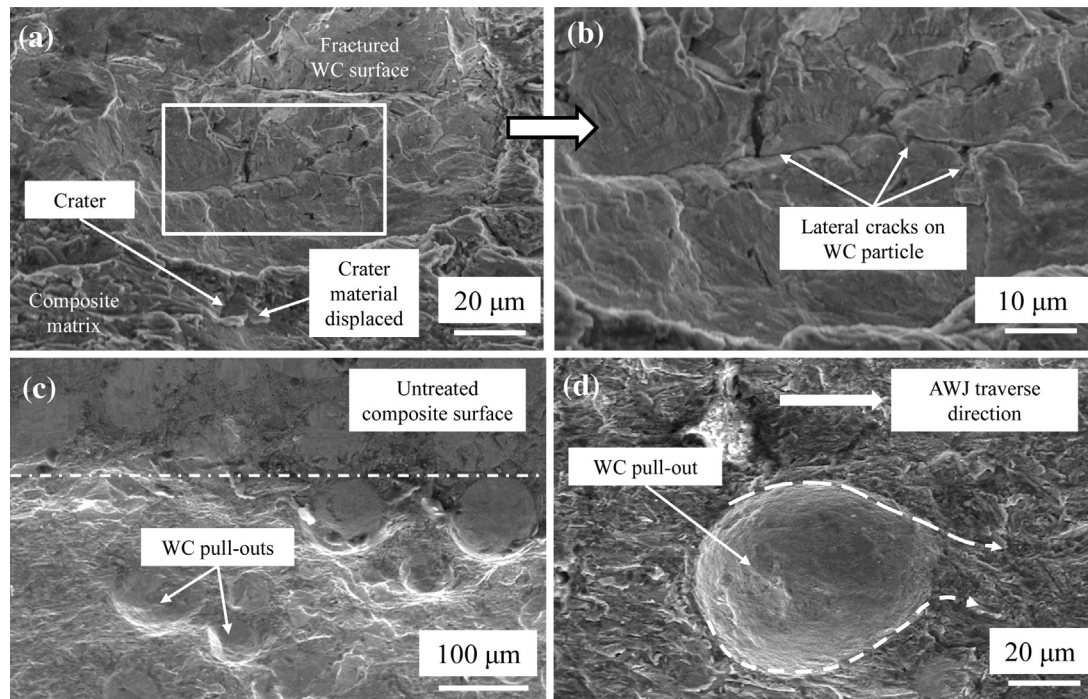


Fig. 8. Micrographs of AWJ impact damage on Ti-6Al-4V/WC composite set A obtained from surface treated with 207 MPa pressure, 200 mm/min traverse speed, 3 mm stand-off distance, and 0.39 g/s abrasive particle feed rate.

in significant material loss on the composite with erosion rates ranging from $\sim 25 \text{ mm}^3/\text{min}$ to $\sim 280 \text{ mm}^3/\text{min}$. In light of this, for AWJ applications, the proposed Ti-6Al-4V/WC composite may only be used for masking low erosion-resistant materials.

The erosion of the Ti-6Al-4V/WC composite increased due to the simultaneous action of the high energy water droplet and accelerated garnet particles. Since, the abrasive particles entrained in the high energy jet travels at a slower speed of 0.7 of water droplet speed (Roth et al., 2005), it is anticipated that the erosion of the surface will be in two stages. Firstly, the water droplet impacts would result in pitting and formation of deep cavities on the composite surface, while the abrasive particle impacts lastly erode the surface. Fig. 8 shows the micrographs of damage associated with AWJ on the Ti-6Al-4V/WC composite. A ploughing effect of the abrasive particle impact on the composite matrix was observed which is indicative of the action of a spherical particle impact on a ductile material (Ruff and Wiederhorn, 1979). Small craters were observed with crater materials displaced in the direction of the particle incidence (Karelin et al., 2002). This crater material is envisaged to fracture off at high strain.

Despite, the uniform distribution of TiC and W reaction products in the β -Ti phase, the composite matrix exhibits a ductile characteristic even at regions near the embedded WC particles. Lateral cracks were seen on the WC particles which had resulted from the direct impact of abrasive garnet at high speed on the WC particles. This was similar to result presented by Lathabai and Pender (1995) and Gant and Gee (2009). In theory, since the abrasive particles employed have spherical morphology, the impact of the abrasive on the WC particles would first result in Hertzian cracks followed by radial cracks, provided that the contact force at impact exceeds a particular threshold value which is material property dependent. The radial cracks formed are responsible for strength degradation, and these cracks propagate to the WC particle surface as lateral cracks which are responsible for chip formation and erosion loss (Ruff and Wiederhorn, 1979).

Craters signifying WC pull-out were seen on the AWJ treated surfaces. As earlier observed that PWJ causes pitting and cavities on

the composite with preferential denudation of the particle/matrix interface dominated by TiC reaction layer, this makes it easier for WC particles to be knocked out of their location by the high velocity abrasive particles. Fig. 7 shows that as the pressure applied on water increases, there was a significant material loss in wrought Ti-6Al-4V when compared to the composite, which indicates the resistance offered by the embedded WC particles and the reaction products reinforcing the composite matrix. It was noted that the erosion loss in the wrought Ti-6Al-4V was fairly similar as the stand-off distance increase, which had resulted in a higher resistance for the composite when the SOD was 3 mm compared to when it was 10 mm. The increase in composite material loss at higher stand-off distance can be attributed to the increased effectiveness of the water droplets and increased potential energy of the abrasive particles in the main region of the flowing jet as explained by Leu et al. (1998). The 3 mm SOD is considered to be in the region of the initial region of the water jet, where the jet is considered as a continuous flow stream which has not been fully discretized into more energetic water droplets. However, at 10 mm SOD, the flowing stream is suggested to have been fully atomised into packets of accelerated droplets which results in a higher water hammer pressure on impact, thus causing increased erosion loss of the composite. The performance of the composite is also significant under the AWJ impacts and the dominating erosion mechanisms are composite matrix ploughing, particle fracture and lateral cracks resulting into chipping.

3.4. Profiles

Fig. 9 compares the mean profiles of cross-sections of the PWJ-resulted kerfs on Ti-6Al-4V and the Ti-6Al-4V/WC composites. The response of these materials under PWJ impacts can be clearly observed. Although material loss from Ti-6Al-4V/WC composites is much less than that from Ti-6Al-4V, there is a noticeable material removal from all composites. It should also be noted that the erosion depths on the Ti-6Al-4V within the waterjet conditions are less than $300 \mu\text{m}$. It is expected that a higher energy density

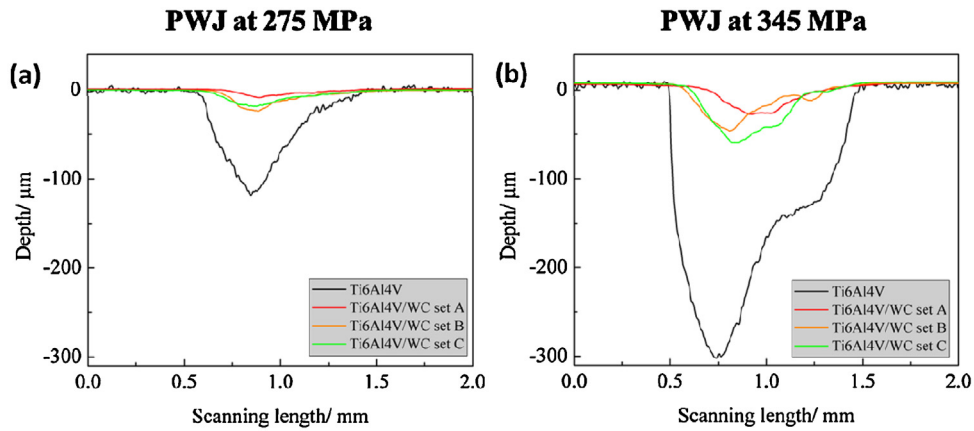


Fig. 9. Mean wear profiles on Ti6Al4V and Ti6Al4V/WC composite resulting from PWJ impacts at SOD=3 mm, $v_t=20$ mm/min and pressures (a) $P_h=275$ MPa; and (b) $P_h=345$ MPa.

of the jet is required to achieve a through cutting of a Ti-6Al-4V material with thickness higher than 300 μ m. Also, there would be a consequential increase in material loss from the Ti-6Al-4V/WC mask should it be exposed to jets with higher energy density. In light of this, the Ti-6Al-4V/WC composite proposed as masking material can be more effectively used in PWJ cutting applications when the target material has a low erosion resistance or in surface treatment of more erosion resistant materials where no significant material removal is required, such as surface roughening and patterning.

3.5. Masking

In order to validate the performance of the clad Ti-6Al-4V/WC composite proposed as masking material in a real manufacturing process, a selective-milling trial was carried out on an aluminium plate using PWJ with the Ti-6Al-4V/WC composite proposed as the mask to create a pocket with a designed pattern. The Ti-6Al-4V/WC composite was laser-deposited on Ti-6Al-4V substrate with a total height of ~ 10 mm. The mask was cut by EDM wire cutting to form the desired milling pattern as shown in Fig. 10. The Ti-6Al-4V/WC

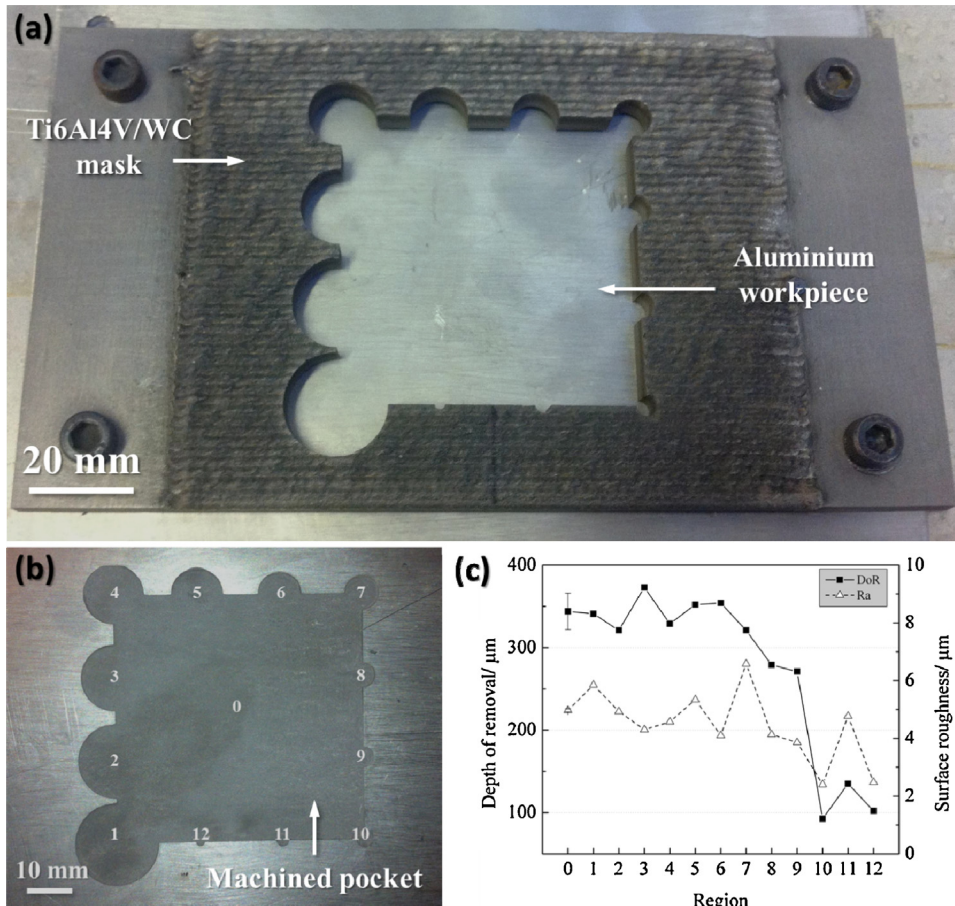


Fig. 10. (a) Demonstrator mask on an aluminium plate. (b) Pocket created using plain waterjet and the mask. (c) Depth of removal and surface roughness in different locations in pocket.

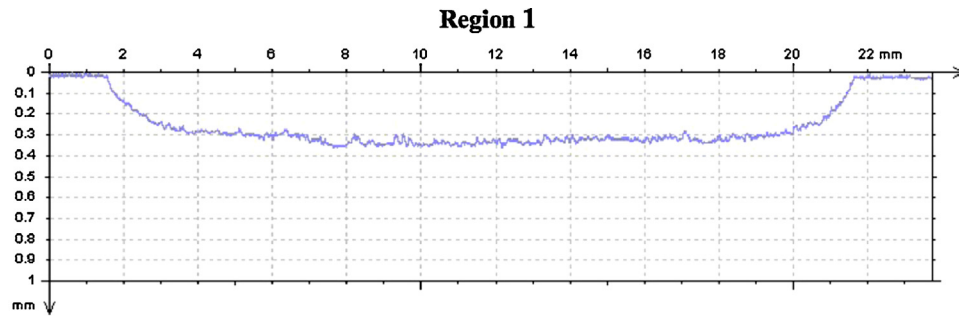


Fig. 11. Linear profile of region 1 showing sharp top corners and edge curvature.

mask was used in the as-deposited form without grinding the surface. PWJ was applied for the milling using a fan jet nozzle optimised for high quality surface finish in machined features. The fan jet nozzle has an elliptical exit profile with its major and minor diameters as $456\ \mu\text{m}$ and $312\ \mu\text{m}$ respectively, and a spraying angle of $32 \pm 1^\circ$. The machining parameters are listed in Table 3.

The pocket created on aluminium plate by PWJ with a Ti6Al4V/WC mask is shown in Fig. 10(b). The sharp edge of the removed area, with only minimal curvature still present indicates good masking performance in terms of defining the pattern of the machining area.

Fig. 11 shows a linear profile of region 1 of the demonstrator piece. A sharp top corner can be seen, reflecting the good adherence to intended geometry, however edge curvature is still present, and in this example extends 2 mm from the top edges. In order to investigate the uniformity in removal depth and roughness of the resulted surface, the machined area is divided into 13 regions of interest. Fig. 10(c) shows the measured removal depth and surface roughness of the defined regions. The depth of removal for region 0 was $344\ \mu\text{m}$ with a standard deviation of $22\ \mu\text{m}$, while the surface roughness (Ra) was determined as $4.97\ \mu\text{m}$ with a standard deviation of $0.05\ \mu\text{m}$. The removal depths of region 1–7 were distributed within bounds of error of the depth of region 0. However, a significant reduction in removal depth can be observed for regions 8–12. The reduction in the material depth removal as the hemispherical pocket size decreases from regions 8–12 can be attributed to the inability of the fan jet nozzle to produce a fine jet of energised water droplets capable of aggressive material removal to the depth between $300\ \mu\text{m}$ and $400\ \mu\text{m}$ as experienced in other regions. Since these pockets are small and are at the edge of the milled pattern, it is suggested that these regions are subjected to droplets in the water mist zone of the jet impinging on the surface. Leu et al. (1998) explained that the water mist zone is the region with droplets considered to have zero velocity which is at the boundary of the energised droplet zone in the main region of the waterjet in air. In this study, the interaction of the near zero velocity, water mist zone droplets with the aluminium surface in these small hemispherical pockets result in small material depth removal and slightly eroded surface with low roughness. The maximum Ra was observed as $6.6\ \mu\text{m}$ in region 7, while region 10 has the minimum Ra of $2.4\ \mu\text{m}$. Irrespective of the different regions over the milled surface, the

standard deviations of removal depth and surface roughness for the whole surface are $100\ \mu\text{m}$ and $1.2\ \mu\text{m}$, respectively.

4. Conclusions

In comparison to Ti-6Al-4V, the proposed Ti-6Al-4V/WC composite exhibited much higher erosion resistance with erosion rates up to 1/13 and 1/8 of that of Ti-6Al-4V under the same erosion conditions in PWJ and AWJ impingement respectively. The composite suffered erosion loss under the action of PWJ by formation of erosion pits, tunnel and deep cavities especially around the WC/matrix interface, while ploughing of the composite matrix, lateral cracking and chipping of embedded WC particles, and WC pull-out characterise the erosion mechanism of the composite under AWJ impact. The overall performance of the Ti-6Al-4V/WC composite is attributed to the embedded WC particles and the uniformly distributed nano-sized reaction products (TiC and W) reinforcing the ductile β -Ti composite matrix.

The demonstration of selective milling of aluminium using Ti-6Al-4V/WC mask indicated that PWJ using a fan jet nozzle resulted in a little damage of the mask while the pocket created on the aluminium had an overall depth of $344\ \mu\text{m}$. The geometry of the mask shape was replicated accurately in the workpiece, however some curvature at the edge of the pocket was still evident.

Further work should aim to further reduce the edge curvature effect. One method proposed is to perform a grinding operation on the clad and then reverse the mask so that the clad is in direct contact with the workpiece, although this method would be restricted when using the cladding process on curved or complex shaped masks. It is anticipated that if these two surfaces can be firmly secured under the action of the jet, the curvature profile at the milled edges could be eliminated. The integrity of the Ti-6Al-4V/WC mask would also be preserved as it would not be directly exposed to jet impacts as well as the reflected jet and the lateral outflow jet.

Acknowledgements

The authors would like to thank Mr. Stuart Branston and Mr. Barry Holdsworth for their invaluable technical contributions during the laser and waterjet experiments in the course of this research.

References

- Adler, W.F., 1979. The mechanics of liquid impact. In: Preece, C.M. (Ed.), *Treatise on Materials Science and Technology*. Academic Press, pp. 127–183.
- Ayers, J.D., 1984. Wear behavior of carbide-injected titanium and aluminum alloys. *Wear* 97, 249–266.
- Castberg, T.S., Johnsen, R., Berget, J., 2013. Erosion of hardmetals: dependence of WC grain size and distribution, and binder composition. *Wear* 300, 1–7.
- Chaudhri, M.M., Walley, S.M., 1978. A high-speed photographic investigation of the impact damage in soda-lime and borosilicate glasses by small glass and steel spheres. *Fracture Mechanics of Ceramics* 3, 349–364.

Table 3
Experimental waterjet conditions for the PWJ mask-milling demonstration.

Nozzle	Fan jet nozzle
Water pressure, MPa	276
Standoff distance, mm	24.5
Jet traverse speed, mm/min	2100
Number of passes	16
Time to finish, mins	200
Step-over distance, mm	1

- Chen, Y., Liu, D., Li, F., Li, L., 2008. WCp/Ti-6Al-4V graded metal matrix composites layer produced by laser melt injection. *Surface and Coatings Technology* 202, 4780–4787.
- Farayibi, P.K., Folkes, J., Clare, A., Oyelola, O., 2011. Cladding of pre-blended Ti-6Al-4V and WC powder for wear resistant applications. *Surface and Coatings Technology* 206, 372–377.
- Farayibi, P.K., Folkes, J.A., Clare, A.T., 2013. Laser deposition of Ti-6Al-4V wire with WC powder for functionally graded components. *Materials and Manufacturing Processes* 28, 514–518.
- Field, J.E., 1999. ELSI conference: invited lecture: Liquid impact: theory, experiment, applications. *Wear* 233–235, 1–12.
- Finnie, I., 1960. An experimental study of erosion. *Proceedings of Society of Experimental Stress Analysis* 17, 65–70.
- Flow, 2013. Dynamic Waterjet XD. <http://www.flowwaterjet.com/en/waterjet-cutting/accessories/dynamic-xd.aspx>
- Folkes, J.A., Shibata, K., 1994. Laser cladding of Ti-6Al-4V with various carbide powders. *Journal of Laser Applications* 6, 88–94.
- Gant, A.J., Gee, M.G., 2009. Structure–property relationships in liquid jet erosion of tungsten carbide hardmetals. *International Journal of Refractory Metals and Hard Materials* 27, 332–343.
- Huang, L., Folkes, J., Kinnell, P., Shipway, P.H., 2012. Mechanisms of damage initiation in a titanium alloy subjected to water droplet impact during ultra-high pressure plain waterjet erosion. *Journal of Materials Processing Technology* 212, 1906–1915.
- Ion, J.C., 2005. *Laser Processing of Engineering Materials. Principle, Procedure and Industrial Application*. Elsevier Butterworth Heinemann, Linacre House, Jordan Hill, Oxford, UK.
- Kamkar, N., Bridier, F., Bocher, P., Jędrzejowski, P., 2013. Water droplet erosion mechanisms in rolled Ti-6Al-4V. *Wear* 301, 442–448.
- Karelin, V.Y., Denisov, A.I., Wu, Y.L., 2002. Fundamentals of hydroabrasive erosion theory. In: Duan, C.G., Karelin, V.Y. (Eds.), *Abrasive Erosion and Corrosion of Hydraulic Machinery*. Imperial College Press, London, pp. 1–51.
- Kong, M.C., Axinte, D., Voice, W., 2010. Aspects of material removal mechanism in plain waterjet milling on gamma titanium aluminide. *Journal of Materials Processing Technology* 210, 573–584.
- Kong, M.C., Axinte, D., Voice, W., 2011. An innovative method to perform maskless plain waterjet milling for pocket generation: a case study in Ti-based superalloys. *International Journal of Machine Tools and Manufacture* 51, 642–648.
- Lathabai, S., Pender, D.C., 1995. Microstructural influence in slurry erosion of ceramics. *Wear* 189, 122–135.
- Leu, M.C., Meng, P., Geskin, E.S., Tismeneskiy, L., 1998. Mathematical modeling and experimental verification of stationary waterjet cleaning process. *Journal of Manufacturing Science and Engineering – Transactions of ASME* 120, 571–579.
- Momber, A., Kovacevic, R., 1996. Fracture of brittle multiphase materials by high energy water jets. *Journal of Materials Science* 31, 1081–1085.
- Momber, A.W., Kovacevic, R., 1999. An energy balance of high-speed abrasive water jet erosion. *Proceedings of the Institution of Mechanical Engineers, Part J: Journal of Engineering Tribology* 213, 463–472.
- Nanduri, M., Taggart, D.G., Kim, T.J., 2000. A study of nozzle wear in abrasive entrained water jetting environment. *Journal of Tribology* 122, 465–471.
- Pugsley, V.A., Allen, C., 1999. Microstructure/property relationships in the slurry erosion of tungsten carbide–cobalt. *Wear* 225–229 (Part 2), 1017–1024.
- Roth, P., Looser, H., Heiniger, K.C., Bühler, S., 2005. Determination of abrasive particle velocity using laser-induced fluorescence and particle tracking methods in abrasive water jets. In: 2005 WJTA American Waterjet Conference, Houston, Texas.
- Ruff, A.W., Wiederhorn, S.M., 1979. Erosion by solid particle impact. In: Preece, C.M. (Ed.), *Treatise on Materials Science and Technology*. Academic Press Inc. Limited, London, pp. 69–124.
- Shipway, P.H., Gupta, K., 2011. The potential of WC-Co hardmetals and HVOF sprayed coatings to combat water-droplet erosion. *Wear* 271, 1418–1425.
- Summers, D.A., 1995. *Waterjetting technology*. Alden Press, Oxford, UK.
- Toyserkani, E., Khajepour, A., Corbin, S., 2005. *Laser Cladding*. CRC Press, Florida, USA.
- Upadhyaya, G.S., 1998. *Cemented Tungsten Carbides: Production, Properties and Testing*. Elsevier Science.
- Vreeling, J.A., Ocelik, V., De Hosson, J.T.M., 2002. Ti-6Al-4V strengthened by laser melt injection of WCp particles. *Acta Materialia* 50, 4913–4924.
- Wang, J., Wong, W.C.K., 1999. A study of abrasive waterjet cutting of metallic coated sheet steels. *International Journal of Machine Tools and Manufacture* 39, 855–870.
- Welsch, G., Boyer, R.F., Collings, E.W., 1994. *Materials properties handbook: titanium alloys*. ASM International. The Materials Information Society.
- Wentzel, E.J., Allen, C., 1995. Erosion-corrosion resistance of tungsten carbide hard metals with different binder compositions. *Wear* 181–183, 63–69, Part 1.
- Yarrapareddy, E., Kovacevic, R., 2008. Synthesis and characterization of laser-based direct metal deposited nano-particles reinforced surface coatings for industrial slurry erosion applications. *Surface and Coatings Technology* 202, 1951–1965.
- Zheng, J.Y., Kim, T.J., 1996. An erosion model of polycrystalline ceramics in abrasive waterjet cutting. *Wear* 193, 207–217.